Drone Power Systems Design Guide

Abstract

This design guide is for modern drone platforms, focusing on the integration of battery management, circuit protection, motor control, and inverter design. It explains how lithium-polymer battery packs combine with an intelligent battery management system, instrumentation, and solid-state circuit protection to meet safety, efficiency, cost, and reliability requirements. An integrated motor controller & driver enables high-performance propulsion using field-oriented control of a permanent magnet synchronous motor. A detailed design example of a delivery drone ties these subsystems together, illustrating practical tradeoffs in power sizing, thermal management, and efficiency. Overall, the document demonstrates how tightly integrated solutions can reduce complexity, weight, and development time while enabling robust, high-performance drone designs.

1. Introduction

Drones incorporate an amazing assortment of systems and technology into small, lightweight frames. Drone applications have expanded far beyond hobby toys to include public safety, agriculture, and commercial uses. Drones will continue finding their way into new and useful roles for the foreseeable future. An enabling factor is the rapid increase in lithium-based battery performance and availability.

Fig. 1-1. Drone power systems

The drone in Fig. 1-1 highlights systems covered in this application note. The battery is comprised of cells connected in series, usually 2 to 14 in series (2S to 14S). Qorvo battery management systems (BMS) are configurable and support a wide cell voltage range to work with any battery chemistry. Power Application Controller® (PAC) motor control and driver (MCD) solutions directly drive the gates of power transistors in half-bridge, full-bridge, or 3-phase bridge configurations. Battery and power management solutions are described first, then MCD for propulsion. Finally, a detailed design example of a delivery drone incorporates these Qorvo solutions.

2. Battery Management

Lithium-polymer is a common battery type for drones. Battery cells are series-connected to achieve the desired battery pack voltage and energy capacity. Common battery pack configurations range from 2S to 8S for hobby drones, and 10S to 14S for payload drones. Cell voltage ranges from about 3 to 4.2 V, with 3.7 V nominal when partially charged.

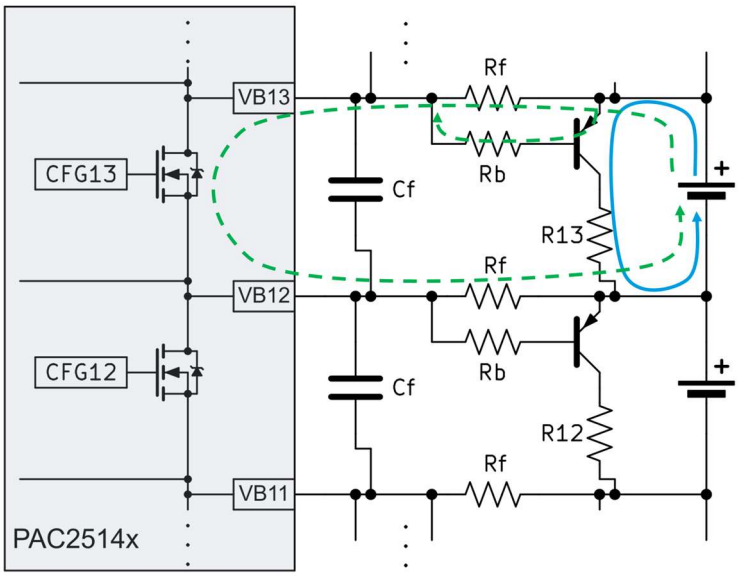

Fig. 2-1. PAC2514x external cell balancing circuit

Higher cell count increases the likelihood of cell charge mismatch with corresponding cell voltage mismatch. Cells with lower-than-average voltage not only shorten runtime, but cells with higher voltage could overcharge, which is extremely hazardous for lithium-based batteries. Preventing charge imbalance requires intelligence within a high cell count battery pack. Each Qorvo PAC BMS provides a simple solution by alternately partially discharging energy in higher voltage cells, with heat dissipated in power transistors and resistors. This process is configurable and can happen anytime, but balancing usually happens during battery charging to maximize runtime. The flagship BMS is the PAC25140 with a 150 MHz Arm® Cortex®-M4F microcontroller core, power management, gate drive, and signal conditioning in a single, small package. External communication is flexible, with 3x USART (either SPI or UART), I^2C/SMBus, and CAN 2.0B peripherals.

Protection features include automatic detection and disconnect in the event of overcurrent, short circuit, battery voltage out of range, and overtemperature. Integrated power management includes a 145 V buck DC-DC controller, 5 and 3.3 V linear regulators, and integrated charge pumps for driving gates of external breaker/disconnect MOSFETs.

A detailed cell balancing example is in [1], and further information is available in [2] and the PAC25140 evaluation kit.

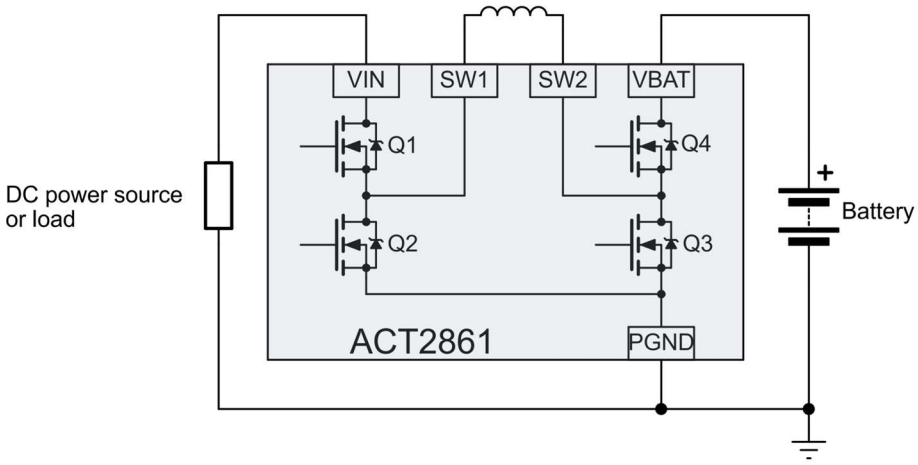

Fig. 2-2. ACT2861 with four internally driven MOSFETs that enable bidirectional power flow and overlapping voltage ranges

For 2S to 5S battery packs, the ACT2861 provides battery disconnect, circuit breaker, and configurable charge and discharge control. The key feature of the ACT2861 is allowing overlapping input and output voltage ranges, and because of this, it is also useful as a general purpose, power management integrated circuit (PMIC) with high current capability, up to 10 A input/output. For example, suppose a load circuit runs on 12 V. With its four internal MOSFETs, the ACT2861 can supply a steady 12 V to the load by seamlessly transitioning from buck to boost mode as the battery voltage decreases from 12.6 V to about 9 V when fully depleted. The ACT2861 is fully configurable by resistors and/or I^2C interface. A detailed design example is available in [3] and the ACT2861 evaluation kit.

3. Motor Control and Drive

Small hobby drones typically use brushless DC (BLDC) or even brushed DC motors. These drones require only speed control, and they prioritize minimal cost, so BLDC without rotor position sensing is an obvious choice. Only three wires interconnect the motor to the electronic speed controller (ESC). Larger drones such as commercial, delivery, and agricultural drones prioritize performance. A permanent magnet synchronous motor (PMSM) with field-oriented control (FOC) delivers maximum torque and efficiency for a given motor size, weight, and current. FOC requires motor current sensing and optionally rotor position sensing. The current measurements are best made near the motor to minimize interference from electrical noise, so an ESC is often bundled with each motor.

In any case, Qorvo motor controllers and drivers (MCDs) are well suited for drones thanks to consolidated functions that minimize space and weight. The PAC system-on-chip platform integrates either a 50 MHz Arm® Cortex®-M0 or 150 MHz Arm® Cortex®-M4F microcontroller core, power management, gate drive, and signal conditioning in a single, small package. Each function is fully tuned and qualified. Qorvo can provide UL / IEC IEC60730 Class B pre-certified firmware to facilitate system-level certification. Particularly useful is the wide operating voltage range without the need for separate, isolated gate drivers.

A detailed battery management and motor control design example is included in [1]. The video [4] goes together with [5]. See [6] for guidance on selecting a part number.

4. Design Example

4.1. Overview

A survey of existing drone designs and their performance yields interesting insight into what is reasonable to expect for this paper design. Fig. 4-1(a) shows flight time versus payload for various commercially available drone designs. The designs vary greatly in payload, battery capacity, empty weight, and end use. The battery configuration is either 12S or 14S lithium-polymer for each drone. Dashed lines are for drones with eight propellers, whereas solid lines are for quadcopters. The Cargo, 30 kg drone with shorter flight time (green dashed line) is a quadcopter configuration but with dual, coaxial propellers on each boom.

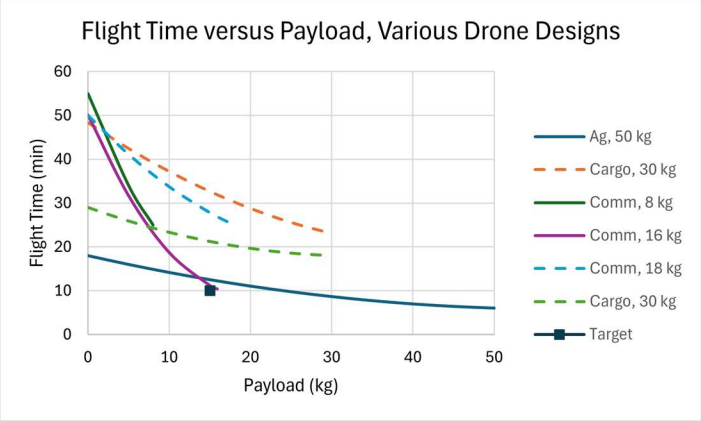

(a)

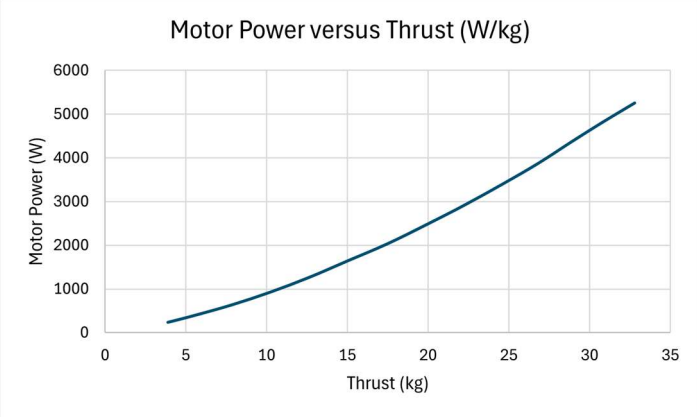

(b)

Fig. 4-1. (a) Flight time versus payload for agricultural, cargo, and commercial drones, (b) single motor + propeller power versus thrust

This design example is for a quadcopter drone capable of carrying a 15 kg payload for 10 minutes, as indicated by the black square marker in Fig. 4-1(a). For the drones surveyed, the drone plus battery mass versus payload ratio *roughly* equals the 1.5. Using this factor, our empty cargo drone plus battery mass is 1.5·15 kg = 22.5 kg, and 37.5 kg total including a 15 kg payload. The fully loaded drone needs a thrust to weight ratio (TWR) of 2 for effective climbing, control, and maneuverability. Thrust versus propeller power is nonlinear, so we need data from a PMSM plus propeller combination, an example of which is shown in Fig. 4-1(b) for model A12KV86 PMSM and MF4114P propeller from T-Motor. At TWR = 2, each motor must output about 2243 W for 18.75 kg thrust per propeller.

Our cargo drone will not always operate at TWR = 2, nor at TWR = 1 (hovering in still air). Assuming an average TWR = 1.2, total thrust is about 45 kg, or 11.25 kg per propeller, requiring 1090 W per propeller. With a 12S lithium-polymer battery at 3.7 V nominal per cell, the nominal battery voltage is 44.4 V. Maximum and minimum battery voltages are 12·4.2 = 50.4 V and 12 · 3 = 36 V respectively. The total battery energy required is 726 Wh, or about 16 Ah. It is unreasonable to use 100% battery capacity with each flight. To accommodate wind, elevation, temperature, battery service life, and some reserve energy, we limit battery discharge to 50% of ideal conditions. For example, a typical flight on a calm day near sea level could start with 80% state of charge and finish with 30%. This means that we need about 32 Ah nominal battery capacity.

4.2. Power MOSFET Selection and Configuration

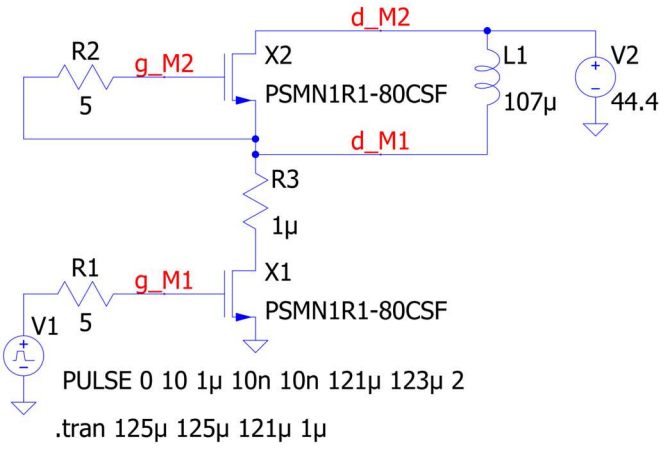

(a)

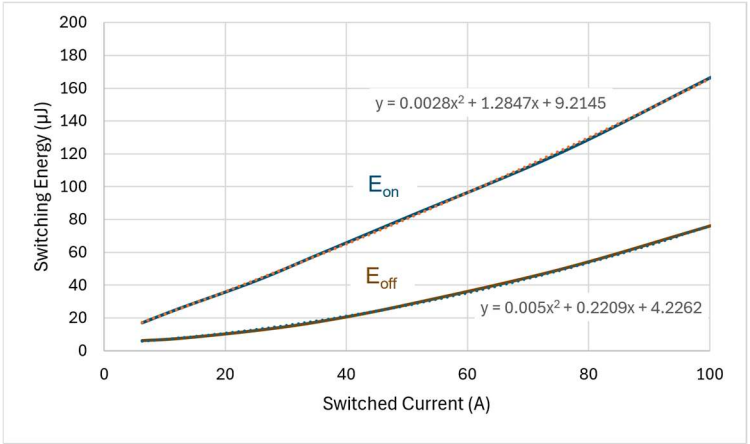

(b)

Fig. 4-2. (a) Inductive switching simulation schematic, (b) PSMN1R1-80CSF switching energy versus current

Choosing an inverter configuration is reminiscent of a driver's license test, choosing the best of multiple seemingly correct answers. We navigate this by following best practices. We begin with a ratio of about 0.67 for applied versus rated MOSFET voltage, so we can

consider MOSFETs with a voltage rating of 80 V or higher. The current is high, so we need a low resistance MOSFET. Top-side cooling is desirable for this high-power drone example. (A power module is not considered here due to weight and cost.) Two good candidates (among others) are PSMNR90-80CSF and PSMN1R1-80CSF from Nexperia.

To help estimate the power loss in each MOSFET, an inductive switching QSPICE simulation using the PSMN1R1-80CSF SPICE model, schematic shown in Fig. 4-2(a), yields switching energy versus current curves shown in (b). The same simulations were made using the PSMNR90-80CSF SPICE model with similar results. These switching energy data go into a power loss calculator [7].

A drone motor has inertia and drag to overcome, but no high startup torque as in a power tool or conveyor belt motor. Fig. 4-3 shows motor torque and current versus thrust for each motor + propeller of our quadcopter design.

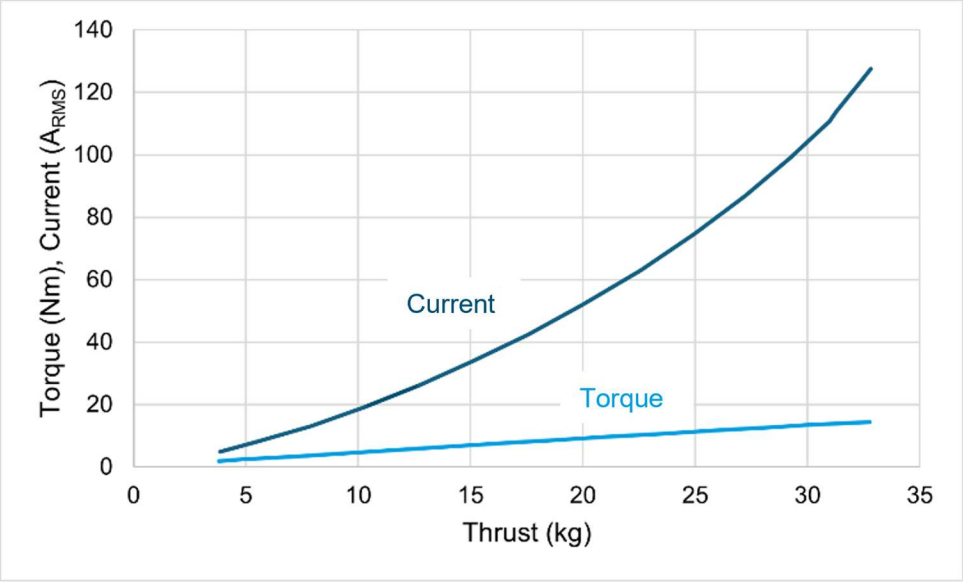

Fig. 4-3. Motor torque and current versus thrust

Torque versus thrust is nearly linear, whereas current increases quadratically due to resistive and core loss in the motor and power loss in the inverter. This combined with switching energy data provides the necessary information to estimate inverter power loss. Calculations with battery voltage = 44.4 V, modulation factor = 1.0 (1.15 is maximum modulation factor, motor line-to-neutral voltage = 15.7 V_{RMS}), motor power = 2243 W (TWR = 2), case-to-sink thermal resistance = 6 °C/W, and heatsink temperature = 85 °C were made with space vector modulation (SVM). The results are shown in Fig. 4-4 comparing the estimated loss of two MOSFETs of the same series but with different chip size.

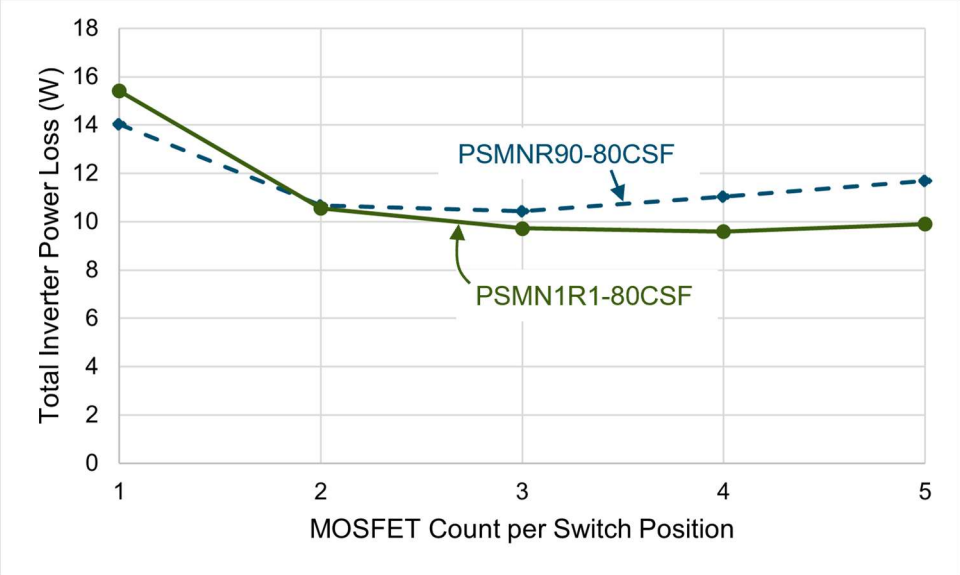

Fig. 4-4. Total inverter power loss versus parallel count per switch position using space vector modulation

For both part numbers, there is a big difference between one versus two parallel MOSFETs per inverter switch position. Power dissipation is reasonable without paralleling. Even with the minimum battery voltage of 36 V and without paralleling, power loss is less than 4 W per MOSFET. However, the loss calculations reveal an important trend. Suppose we need to operate at higher power for several seconds – call it emergency boost mode. The motor + propeller combination can certainly handle higher power (perhaps oversized), but without paralleling, the inverter MOSFETs could go into thermal runaway. With two parallel MOSFETs, current per MOSFET is reduced from 48 A_{RMS} to a much more benign 24 A_{RMS} per MOSFET, assuming nominal battery voltage. It is important to include design margin to accommodate nonuniform current sharing between parallel MOSFETs, and there is ample margin in this case. Paralleling three versus two MOSFETs significantly improves efficiency *per MOSFET*, but total inverter loss is almost flat or even increases with parallel count. With these assumptions, at this power level, paralleling two MOSFETs is the most promising starting point for a real design, especially considering the additional cost and space for higher parallel count.

Fig. 4-4 reveals another interesting trend. The higher $R_{DS(on)}$ MOSFET switches faster, so it has lower switching loss, which offsets its higher conduction loss except at high current (no paralleling). With two or more in parallel, the higher $R_{DS(on)}$ MOSFET efficiency meets or exceeds that of the lower $R_{DS(on)}$, more costly MOSFET. This coincides with the (switch-mode) best practice of paralleling and spreading out heat sources on an air-cooled heatsink, even if a single, lower on-resistance MOSFET could work. With two in parallel per switch position, PSMN1R1-80CSF is the lowest cost option of the two MOSFETs compared here.

With two parallel MOSFETs, the power loss calculator predicts 26% lower total loss per MOSFET using 60° discontinuous modulation (DPWM1) versus SVM [7], [8], [9]. In any case, the inverter efficiency should be quite good, well over 99% considering only power semiconductor losses.

Finally, the main benefit of power loss calculations is to clearly see trends and to focus on configurations with well-balanced tradeoffs, reducing prototype development and testing costs. Accuracy is important, but it is not the main goal of power loss calculations.

4.3. MCD Selection and Configuration

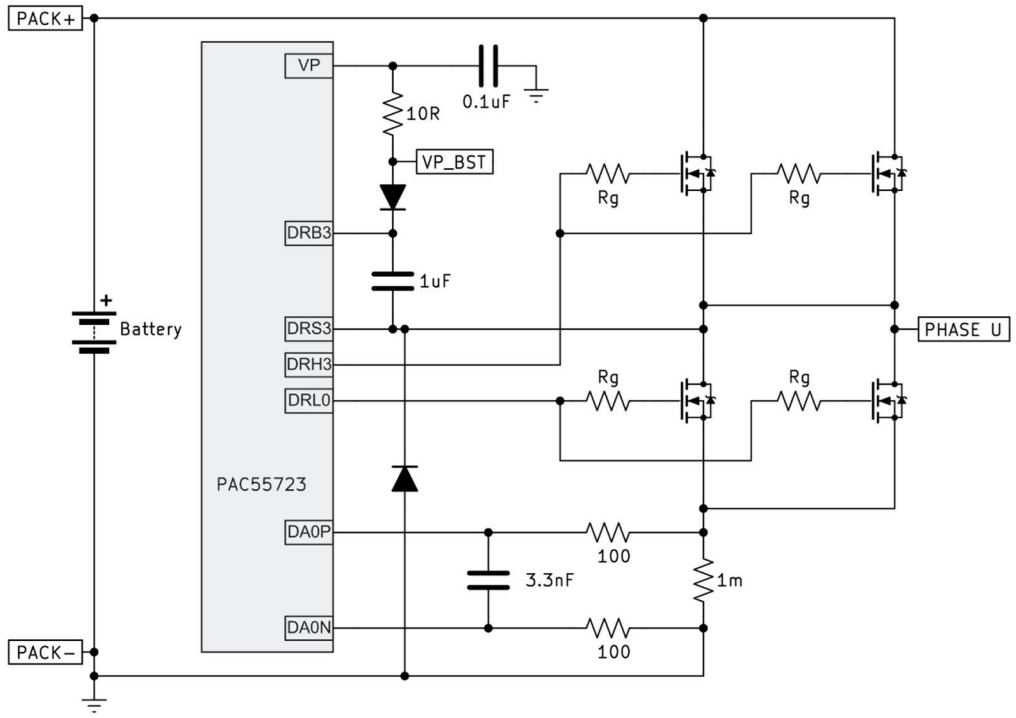

Fig. 4-5. Inverter phase *u* simplified schematic showing PAC55723 gate drive and current sense connections

A good choice for an integrated motor controller and driver is PAC55723. Other choices would work well too, but this one is well suited for field-oriented control of a PMSM with three simultaneous sample-and-hold, three differential programmable gain amplifiers for current sensing, a high clock speed (150 MHz), floating point unit, and hardware multiply and divide. The 72 V absolute maximum input voltage rating is sufficient for many battery voltages. V_{DS} sense (DESAT) is omitted in the PAC55723, but it is arguably not needed for driving a propeller. Finally, lower pin count in a smaller package is a good fit.

Fig. 4-5 shows a simplified schematic with gate drive and current sense connections for one phase leg with two parallel MOSFETs per switch position. Per best practice, each MOSFET has its own gate resistor, or resistors if using a steering diode to separately control switch-on and switch-off speed. A gate resistance of 5 to 10 Ω would be reasonable for initial testing. High-side gate drive power is from a bootstrap for each phase, but node VP_BST is common for all phases. Low-side driver power is from VP.

Gate drive power to switch the inverter MOSFETs is $P_{driver,sw} = Q_{G(tot)} \cdot f_{sw} \cdot \Delta V_{GS}$, where $Q_{G(tot)}$ is the total gate charge from the external MOSFET datasheet, f_{sw} is the switching frequency, and ΔV_{GS} is gate voltage swing of the external MOSFET [1]. This power is lost during switching as heat in resistances in the gate current path, namely the driver MOSFET resistances $R_{dr,h}$ and $R_{dr,l}$, external gate resistance R_G, and gate resistance inside the driven MOSFET $R_{G,int}$. Half the power is lost during switch-on, the other half during switch-off. Power loss in internal gate drive MOSFETs is, by voltage division across the resistances:

$$P_{dr,h} = \frac{1}{2} \cdot Q_{G(tot)} \cdot f_{sw} \cdot \Delta V_{GS} \cdot \frac{R_{dr,h}}{R_{dr,h+R_{G,on}+R_{G,int}}}$$

$$P_{dr,l} = \frac{1}{2} \cdot Q_{G(tot)} \cdot f_{sw} \cdot \Delta V_{GS} \cdot \frac{R_{dr,l}}{R_{dr,l+R_{G,off}+R_{G,int}}}$$

The PAC55723 drives to about 10 V. A chart in the PAC55723 datasheet shows internal driver resistance versus temperature. Choosing 80 °C as the operating temperature, the internal driver on and off resistances are about 10 and 4 Ω respectively. The selected PSMN1R1-80CSF MOSFET has typical internal gate resistance R_G = 1.12 Ω. Typical gate charge per MOSFET is 242 nC, driving between 0 and 10 V, and other test conditions reasonably close to this application. Let R_G = 10 Ω. Internal gate driver MOSFET power losses per driven MOSFET are:

$$P_{dr,h} = P_{dr.l} = \frac{1}{2} \cdot 242\ nC \cdot 20\ kHz \cdot 10\ V \cdot \frac{10\ \Omega}{10\ \Omega + 10\ \Omega + 1.12\ \Omega} = 11.5\ mW$$

$$P_{dr,l} = P_{dr.l} = \frac{1}{2} \cdot 242\ nC \cdot 20\ kHz \cdot 10\ V \cdot \frac{4\ \Omega}{4\ \Omega + 10\ \Omega + 1.12\ \Omega} = 6.4\ mW$$

Summing these and doubling because of two parallel driven MOSFETs, the total internal driver power loss per switch position is 36 mW, and the sum for all six drivers is 216 mW. Thanks to the exposed bottom metal pad on the PAC55723, junction-to-ambient thermal resistance is only 23.4 °C/W, resulting in an estimated temperature rise of about 5 °C due to gate driver power loss.

Peak current at TWR = 2 is about 68 A. A current sense resistor per phase is the lowest cost, smallest volume option. This paper design uses low-side, 1 mΩ, 10 W current sense resistors with a low-inductance design, such as part number SEWF5930D1L00P9 from C&B Electronics. With a 2.5 V full-scale output, the differential amplifier gain in the PAC55723 could be set at 16 while still allowing measurement of current 2x higher than at peak power. Power dissipation in the current sense resistor is the limiting factor, at a practical 2.3 W at TWR = 2.

4.4. Battery Management

The circuit breaker/battery disconnect design is critical in this high-current application, and in fact, it largely determines the drone power configuration. Total power draw with full 15 kg cargo load and TWR = 2 is 4 · 2243 = 9 kW. At minimum battery voltage of 36 V, total current draw is 250 A. The ratio between breaker trip current and this maximum load current should be 1.5 to 2 to avoid false trips. To reduce the size and cost of the breaker/disconnect, this example design uses two battery packs, each containing a BMS controller with breaker/disconnect.

Features that make a solid-state circuit breaker (SSCB) attractive include:

- Flexibility
- Auto or remote reset
- Durability

The current limit is programmable, even in real-time based on telemetry (combination of current slew rate, magnitude, and duration). Surge ride-through while still protecting from fault damage (selectivity) is especially important for aircraft. Arc-free switching eliminates wear that shortens the service life of electro-mechanical breakers.

The main disadvantage of SSCBs is heat generation (power loss). Paralleling trades lower power loss for increased cost and space as well as reduced slew rate control. Limiting the current slew rate is important when switching both on and off. Slow switch-on prevents problematic voltage transients caused by excessive inrush current. A high switch-on gate resistance (hundreds of Ohms) puts the MOSFETs in the SSCB in active mode (partially on) for a thermally significant duration. Parallel MOSFETs are bad at sharing current in active mode due to normal part-to-part variation in transconductance with corresponding threshold voltage variation. Methods to help limit current slew rate include:

- Precharge (soft start) resistor circuit [10]
- Feedback control of each MOSFET current
- Switch SSCB MOSFETs on and off repeatedly until downstream capacitors are charged
- Add an inductor and freewheeling diode to limit inrush current.
- More MOSFETs in parallel, each with high gate resistance

Feedback control of each MOSFET requires an op-amp to drive each MOSFET gate, which is an elegant solution but complex. Paralleling more MOSFETs statistically overcomes the current sharing issue, but at high cost and space. Pulsing is feasible with a PAC25140, the selected BMS controller for this design example. It includes the same 150 MHz, floating point processor as in the PAC55723 MCD. Probably the most straightforward option is a precharge circuit as in [10].

To improve reliability of the slowly switched MOSFETs in the breaker/disconnect, it is best to select ones with a wider safe operating area (SOA), optimized for hot swap and soft start applications. This example design uses top-side cooled PSMN1R0-80CSE from Nexperia. This MOSFET has reduced transconductance (gain), which significantly widens the SOA and reduces the threshold voltage variation (improves current sharing) at the expense of slightly increased $R_{DS(on)}$. We calculate power loss using the same approach as for the motor drive inverters, again with a heatsink temperature of 85 °C, isolating pad thermal resistance of 6 °C/W, and two battery packs with peak load current of 125 A per pack. With three parallel MOSFETs, power loss per MOSFET is 2 W, so 6 W for all three.

Setting the automatic overcurrent trip at 1.5x maximum battery current with TWR = 2 and minimum battery voltage of 36 V, overcurrent trip is set at 188 A. At this current, power loss is a reasonable 4.9 W each, and 14.8 W for all three MOSFETs.

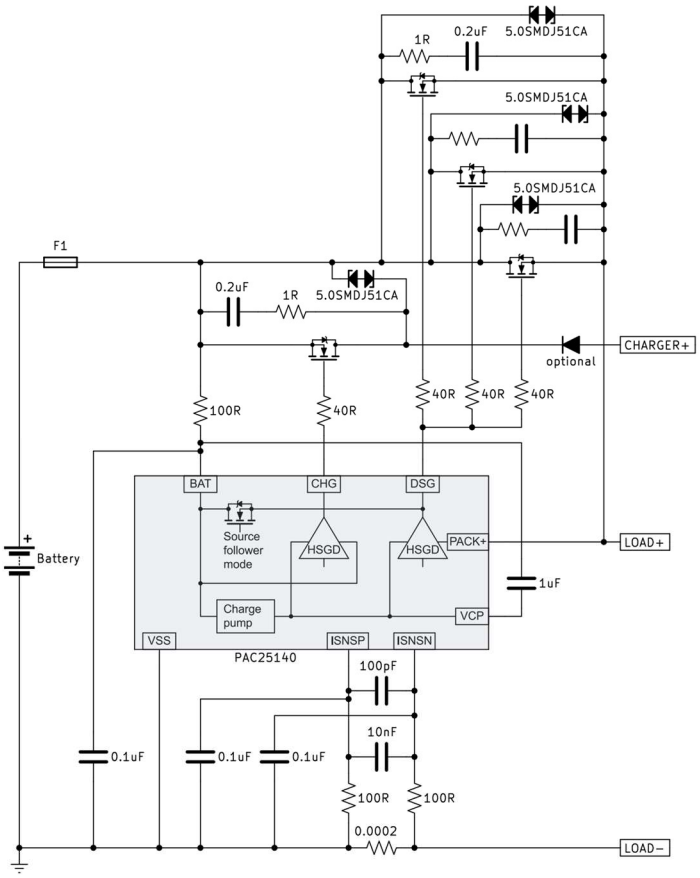

Fig. 4-6. PAC25140 partial block diagram showing circuit breaker/disconnect and current sense connections

The PAC25140 accommodates different discharge versus charge rates by separately driving discharge and charge breaker/disconnect MOSFETs. This reduces power loss by separating the discharge and charge paths so that current flows through only one MOSFET (or set of parallel MOSFETs) instead of two [11]. It also saves cost and space because charge current is typically less than discharge current. In this example design, the charge current is one-third the full-load discharge current of 125 A per battery, so 41.7 A maximum charge current. This is handled by a single PSMN1R0-80CSE MOSFET.

Fig. 4-6 shows a simplified schematic of the breaker/disconnect circuitry around the PAC25140 BMS controller. The three parallel discharge breaker/disconnect MOSFETs each have a gate resistor and drain-source snubber. Individual gate resistors are required, but the snubbers could be combined. There is a separate charge breaker/disconnect MOSFET for a separate charger connection. See [11] for more details. The design omits the self control fuse (SCF) drive feature of the PAC25140 because the currents are too high for an SCF.

A snubber is required, especially when switching off high current. Starting values for testing could be 0.2 µF to 0.25 µF and 1 Ω snubber capacitance and resistance per MOSFET with a gate resistance of 40 Ω per MOSFET [1]. The resistors must be pulse rated. Transient voltage suppressors are included to absorb some of the inductive energy in the event of emergency switch-off.

Current sense is with a 0.2 mΩ resistor. Power dissipation is again the limiting factor, equal to 3.1 W at TWR = 2. With a rating of 15 W, the current sense resistor has almost 5x margin for good reliability. With the programmable amplifier gain in the PAC25140 set to 8, the input sense voltage multiplied by the gain setting remains within the PAC25140 recommended limit of ±0.3 V, even at the overcurrent trip setting.

Separate 16-bit analog-to-digital converters in the PAC25140 enable precise Coulomb counting for battery state of charge and health calculations, and for individual cell voltage monitoring and balancing. The cell balancing concept in PAC2514x BMS controllers is shown in Fig. 2-1 and explained in detail in [1] and [2], so it is not repeated here.

5. Summary

This application note summarizes the key design considerations and practical implementation details for building a drone capable of delivering 15 kg cargo. Systems discussed include battery management, circuit protection, motor control, and inverter design. A detailed design example guides component selection and configuration, and it predicts motor drive inverter and circuit breaker/disconnect performance.

References

[1] J. Dodge, “Outdoor Power Equipment Design Guide,” Qorvo. [Online]. Available: https://www.qorvo.com/products/d/da009838
[2] Application note, “PAC2xxxx External Cell Balancing,” Qorvo. [Online]. Available: https://www.qorvo.com/products/d/da009029
[3] A. Molley, J. Dodge, “Battery Charger and Motor Controller in Roller Blinds,” Qorvo. [Online]. Available: https://www.qorvo.com/design-hub/technical-articles
[4] Qorvo/J. Dodge, *Field-Oriented Control – Permanent Magnet Synchronous Machines*, Accessed: Dec. 5, 2025. [Online Video]. Available: https://www.qorvo.com/design-hub/videos/field-oriented-control-permanent-magnet-synchronous-machines
[5] J. Dodge, “Introduction to Permanent Magnet Motor Control,” Qorvo. [Online]. Available: https://www.qorvo.com/design-hub/technical-articles
[6] J. Dodge, “Qorvo Motor Control & Drive System Guide,” Qorvo. [Online]. Available: https://www.qorvo.com/products/d/da009837
[7] J. Dodge, “Inverter Power Loss Calculation,” Qorvo. [Online]. Available: https://www.qorvo.com/design-hub/technical-articles
[8] J. Dodge, “Introduction to Modulation of 3-Phase Inverters,” Qorvo. [Online]. Available: https://www.qorvo.com/design-hub/technical-articles
[9] D. Graham Holmes, Thomas A. Lipo; “Concept of a Space Vector,” in *Pulse Width Modulation for Power Converters, Principles and Practice*,Piscataway, NJ, USA: IEEE Press / Wiley InterScience, 2003, ch. 1, sec. 1.6, pp. 24-38.
[10] Application note, “Pre-Charge Circuit,” Qorvo. [Online]. Available: https://www.qorvo.com/products/d/da008589
[11] Application note, “PAC2xxxx BMS Parallel FET Operation,” Qorvo. [Online]. Available: https://www.qorvo.com/products/d/da009026
[12] A. Futo, I. Varjasi, I. Vajk, R. K. Jardan, “Analytical Compensation of Harmonics Caused by 60° Flat-Top Modulation,” IET Power Electronics, June 2019

Revision History

Revision	Author	Date	Description
A	Jonathan Dodge, P.E.	10 March 2026	Initial draft

Contact Information

For the latest specifications, additional product information, worldwide sales and distribution locations:

Web: www.qorvo.com

Tel: +1 844-890-8163

Email: customer.support@qorvo.com

Important Notices

The information contained in this Document and any associated documents ("Document Information") is believed to be reliable; however, Qorvo makes no warranties regarding the Document Information and assumes no responsibility or liability whatsoever for the use of or reliance on said information. All Document Information is subject to change without notice. Customers should obtain and verify the latest relevant Document Information before placing orders for Qorvo® products. Information concerning Qorvo's product life cycles is available at https://www.qorvo.com/support/product-lifecycle-information. Document Information or the use thereof does not grant, explicitly, implicitly or otherwise any rights or licenses with respect to patents or any other intellectual property whether with regard to such Document Information itself or anything described by such information.

Qorvo grants you permission to use this Document and any associated resources only to develop an application that uses the Qorvo products described in the Document and any associated resources. Other reproduction and display of this Document and any associated resources is prohibited.

Qorvo's products are provided subject to Qorvo's Terms of Sale or provided in conjunction with such Qorvo products. Qorvo objects to and rejects any additional or different terms customer may have proposed regarding the purchase of Qorvo products.

APPLICATION NOTE INFORMATION DOES NOT CONSTITUTE A WARRANTY WITH RESPECT TO THE PRODUCTS DESCRIBED HEREIN, AND QORVO HEREBY DISCLAIMS ANY AND ALL WARRANTIES WITH RESPECT TO SUCH PRODUCTS WHETHER EXPRESS OR IMPLIED BY LAW, COURSE OF DEALING, COURSE OF PERFORMANCE, USAGE OF TRADE OR OTHERWISE, INCLUDING THE IMPLIED WARRANTIES OF MERCHANTABILITY AND FITNESS FOR A PARTICULAR PURPOSE. Without limiting the generality of the foregoing, Qorvo® products are not warranted or authorized for use as critical components in medical, life-saving, or life-sustaining applications, or other applications where a failure would reasonably be expected to cause severe personal injury or death. Applications described in the Document Information are for illustrative purposes only. Customers are responsible for validating that a particular product described in the Document Information is suitable for use in a particular application.